European Radiology (2019) 29:6163–6171
https://doi.org/10.1007/s00330-019-06170-3

IMAGING INFORMATICS AND ARTIFICIAL INTELLIGENCE

Deep learning reconstruction improves image quality of abdominal ultra-high-resolution CT

Motonori Akagi[1] · Yuko Nakamura[1] · Toru Higaki[1] · Keigo Narita[1] · Yukiko Honda[1] · Jian Zhou[2] · Zhou Yu[2] · Naruomi Akino[3] · Kazuo Awai[1]

Received: 6 January 2019 / Revised: 22 February 2019 / Accepted: 14 March 2019 / Published online: 11 April 2019

Abstract

Objectives Deep learning reconstruction (DLR) is a new reconstruction method; it introduces deep convolutional neural networks into the reconstruction flow. This study was conducted in order to examine the clinical applicability of abdominal ultra-high-resolution CT (U-HRCT) exams reconstructed with a new DLR in comparison to hybrid and model-based iterative reconstruction (hybrid-IR, MBIR).

Methods Our retrospective study included 46 patients seen between December 2017 and April 2018. A radiologist recorded the standard deviation of attenuation in the paraspinal muscle as the image noise and calculated the contrast-to-noise ratio (CNR) for the aorta, portal vein, and liver. The overall image quality was assessed by two other radiologists and graded on a 5-point confidence scale ranging from 1 (unacceptable) to 5 (excellent). The difference between CT images subjected to hybrid-IR, MBIR, and DLR was compared.

Results The image noise was significantly lower and the CNR was significantly higher on DLR than hybrid-IR and MBIR images ($p < 0.01$). DLR images received the highest and MBIR images the lowest scores for overall image quality.

Conclusions DLR improved the quality of abdominal U-HRCT images.

Key Points

- *The potential degradation due to increased noise may prevent implementation of ultra-high-resolution CT in the abdomen.*
- *Image noise and overall image quality for hepatic ultra-high-resolution CT images improved with deep learning reconstruction as compared to hybrid- and model-based iterative reconstruction.*

Keywords Liver · Neural networks (computer) · X-ray computed tomography · Machine learning · Artificial intelligence

Abbreviations

AiCE	Advanced Intelligent Clear-IQ Engine
AIDR3D	Adaptive iterative dose reduction 3-dimensional
CNR	Contrast-to-noise ratio
$CTDI_{vol}$	CT dose index
DCNN	Deep convolutional neural networks
DICOM	Digital Imaging and Communications in Medicine
DLP	Dose-length product
DLR	Deep learning reconstruction
EP	Equilibrium phase
FIRST	Forward-projected model-based iterative reconstruction solution
HAP	Hepatic arterial phase
HU	Hounsfield units
Hybrid-IR	Hybrid iterative reconstruction
MBIR	Model-based iterative reconstruction
PVP	Portal venous phase
ROI	Region of interest
SD	Standard deviation
SSDE	Size-specific dose estimate
U-HRCT	Ultra-high-resolution computed tomography

Electronic supplementary material The online version of this article (https://doi.org/10.1007/s00330-019-06170-3) contains supplementary material, which is available to authorized users.

✉ Yuko Nakamura
yukon@hiroshima-u.ac.jp

[1] Diagnostic Radiology, Hiroshima University, 1-2-3 Kasumi, Minami-ku, Hiroshima, Japan

[2] Canon Medical Research USA, Inc., Vernon Hills, IL, USA

[3] Canon Medical Systems Co. Ltd., Otawara, Japan

Introduction

Ultra-high-resolution computed tomography (U-HRCT), commercially available since 2017, features a smaller detector element and tube focus size than conventional CT. U-HRCT yields images of higher spatial resolution; their usefulness for the examination of the lungs, coronary arteries, and peripheral arteries has been reported [1–4]. However, compared to conventional CT, U-HRCT has greater image noise due to relatively insufficient incident photons on smaller detectors. As a consequence, increased noise may prevent implementation for abdominal examinations [1, 4, 5].

Model-based iterative reconstruction (MBIR) can improve the image quality and potentially reduce radiation dose [6–8]. However, MBIR images are remarkably degraded due to low-frequency noise, particularly at low radiation dose settings [9–12]. In addition, the MBIR approach usually requires higher computational power and longer computational time. Hybrid iterative reconstruction (hybrid-IR) is faster than MBIR. However, the overall imaging performance of hybrid-IR is not as good as of MBIR in terms of the noise characteristics, spatial resolution, and artifact reduction [6, 13–16].

Deep learning reconstruction (DLR) (Advanced Intelligent Clear-IQ Engine [AiCE], Canon Medical Systems) is the first commercialized deep learning reconstruction tool. It incorporates deep convolutional neural networks (DCNN) restoration process into the reconstruction flow. For the deep learning-based approach, given hybrid-IR images and high-dose MBIR images as training pairs, statistical features that differentiate signal from the noise and artifacts could be "learned" in the training process and then be "updated" in the DCNN kernel for future inference use (Fig. 1). As DCNN kernel is trained with ideal MBIR images, we expect to see that not only the DLR approach could generate comparable image quality to the MBIR image but also that it takes shorter processing time than MBIR; therefore, DLR could be useful for reconstructing abdominal U-HRCT images. In this study, we investigated the clinical applicability of DLR and compared its image quality to hybrid-IR and MBIR.

Materials and methods

This retrospective study was approved by our institutional review board; prior informed patient consent was waived because this study used existing CT images including raw data. Patient records and information were anonymized and de-identified prior to analysis.

Study population

We estimated the sample size needed to detect a difference between CT images reconstructed with hybrid-IR, MBIR, and DLR as 20 patients with an effect size of 0.85, an α of 0.013 (one third value of 0.05 because of Bonferroni correction for multiple comparison), and a statistical power of 0.8 [17]. Effect size was calculated based on the preliminary data using images of 10 patients not included in this study.

This study included 46 consecutive patients (31 men, 15 women, age range 34–86 years; mean age, 73 years) who had undergone hepatic dynamic CT using U-HRCT at our institution between December 2017 and April 2018. The clinical indication for hepatic dynamic CT was follow-up after surgery for malignant liver tumor ($n = 25$), evaluation after chemotherapy for a malignant liver tumor ($n = 14$), staging of a suspected malignant liver tumor ($n = 1$), and screening for liver tumors ($n = 6$).

CT image acquisition

Images were acquired on a U-HRCT scanner (Aquilion Precision, Canon Medical Systems). The scanning protocols were as follows: rotation time 0.75 s, pitch factor 0.806, scanning field of view 40 cm, voltage 120 kV, and tube current 250 mA. Hepatic dynamic CT images were obtained during

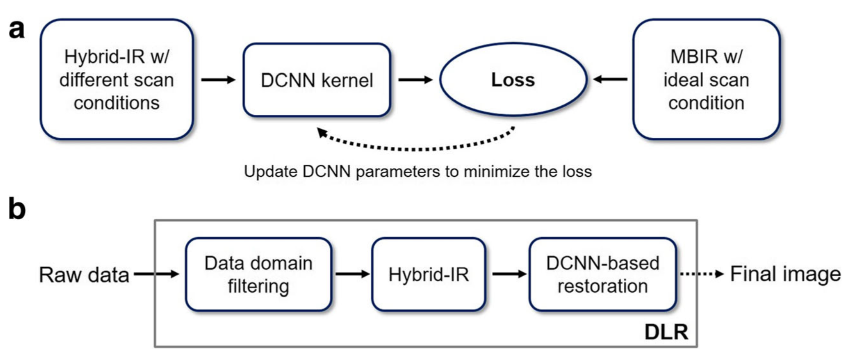

Fig. 1 Training and inference flowchart of deep learning reconstruction (DLR) algorithm. **a** Parameters in the DCNN kernel optimized in the training process when differences (loss) between the DCNN output and the ideal MBIR image are stably minimized. **b** The DLR for the data inference includes three major parts: data domain filtering, hybrid-IR reconstruction, and a DCNN-based restoration module

Table 1 Image noise and CNR on hybrid-IR, MBIR, and DLR images

	Hybrid-IR	MBIR	DLR	*p* values		
				Hybrid-IR vs MBIR	Hybrid-IR vs DLR	MBIR vs DLR
Image noise (HU)						
HAP	24.9 (14.8–46.9)	22.2 (14.5–37.8)	13.9 (10.9–32.5)	< 0.01	< 0.01	< 0.01
EP	25.5 (18.3–40.1)	23.1 (15.9–42.0)	14.6 (10.7–32.8)	< 0.01	< 0.01	< 0.01
CNR at HAP						
Aorta	11.7 (5.5–24.7)	12.7 (6.5–27.8)	19.9 (8.5–35.3)	< 0.01	< 0.01	< 0.01
Portal vein	3.1 (− 0.8 to 6.8)	3.4 (− 0.9 to 7.5)	5.2 (− 1.3 to 12.2)	0.01	< 0.01	< 0.01
Liver	0.7 (− 0.7 to 1.9)	0.8 (− 0.6 to 1.8)	1.2 (− 1.5 to 3.2)	0.31	< 0.01	< 0.01
CNR at EP						
Aorta	2.1 (1.1–4.6)	2.2 (1.1–4.8)	3.3 (1.6–7.5)	0.03	< 0.01	< 0.01
Portal vein	2.2 (1.4–4.8)	2.2 (1.4–5.5)	3.4 (1.9–8.2)	0.02	< 0.01	< 0.01
Liver	1.3 (0.7–2.8)	1.2 (0.4–2.7)	2.0 (0.9–4.6)	0.21	< 0.01	< 0.01

Data are median with ranges in parentheses

HAP hepatic arterial phase, *EP* equilibrium phase

the hepatic arterial and the equilibrium phase (HAP, EP) in super-high-resolution mode (1792 channels per detector row, 0.25 mm × 160 rows; matrix size, 1024) because these phases are essential for diagnosing hepatocellular carcinoma [18–21]. An automatic bolus-tracking program was used to time the start of scanning for each phase after contrast medium injection. The trigger threshold level was set at 200 Hounsfield units (HU) in the abdominal aorta at the L1 vertebral body level. HAP and EP scans were started at 17 and 152 s after triggering. The contrast material (600 mgI/kg body weight) was administered using a power injector (Dual Shot, Nemoto Kyorindo) and a 20-gauge catheter inserted into an antecubital vein. The injection duration was 30 s in all patients and the delivery of contrast material was followed by flushing with 30 mL of physiologic saline at the same injection rate.

Although pre-enhanced and portal venous phase (PVP) scans were obtained for the clinical studies, they were not evaluated in ours because they were not performed in super-high-resolution mode.

To assess radiation exposure, we reviewed the CT dose index ($CTDI_{vol}$) and the dose-length product (DLP) recorded as Digital Imaging and Communications in Medicine (DICOM) data. We also calculated the size-specific dose estimate (SSDE), an index in which the CTDI is corrected by the body habitus [22, 23]. Size-dependent conversion factors were obtained from AAPM Report 204 [24]; they were based on the sum of the anteroposterior and lateral dimensions at the mid-liver level of each patient.

Image analysis

The CT images at HAP and EP were reconstructed with hybrid-IR (Adaptive Iterative Dose Reduction 3-Dimensional [AIDR3D, standard setting]; Canon Medical Systems), MBIR (forward-projected model-based iterative reconstruction solution [FIRST]; Canon Medical Systems), and DLR (AiCE).

Table 2 Qualitative analysis scores of hybrid-IR, MBIR, and DLR images

	Hybrid-IR	MBIR	DLR	*p* values		
				Hybrid-IR vs MBIR	Hybrid-IR vs DLR	MBIR vs DLR
HAP						
Vessel conspicuity	3.50 (0.62)	4.33 (0.56)	3.67 (0.82)	< 0.01	0.08	< 0.01
Overall image quality	2.91 (0.51)	2.59 (0.54)	4.04 (0.51)	< 0.01	< 0.01	< 0.01
EP						
Overall image quality	2.70 (0.55)	2.26 (0.49)	3.63 (0.49)	< 0.01	< 0.01	< 0.01

Data are expressed as mean (standard deviation)

HAP hepatic arterial phase, *EP* equilibrium phase

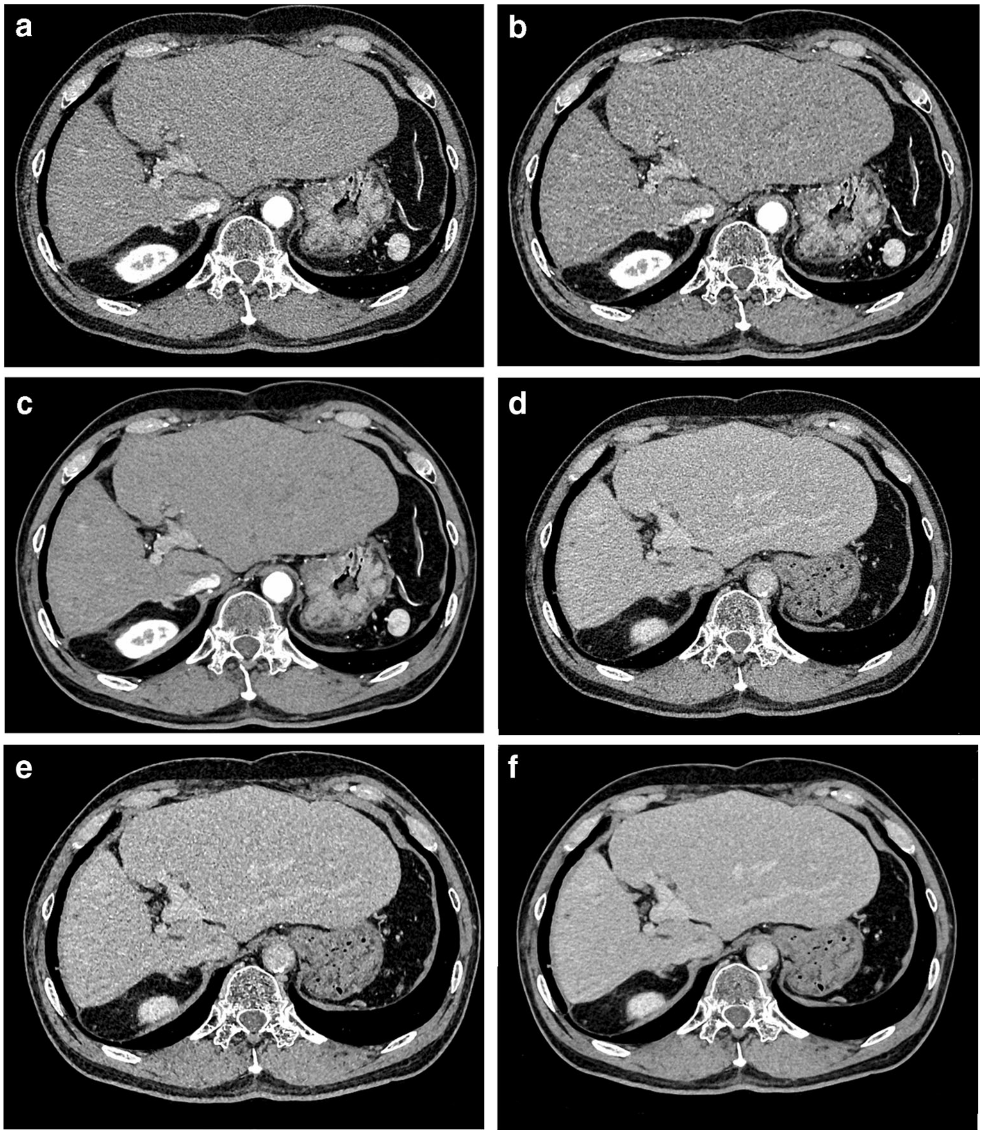

Fig. 2 Hepatic arterial (**a**–**c**) and equilibrium phase images (**d**–**f**) of a 72-year-old woman. Reconstruction was with hybrid-IR (**a**, **d**), MBIR (**b**, **e**), and DLR (**c**, **f**). Compared with the hybrid-IR image, the image noise was not reduced on the MBIR image. On the image reconstructed with DLR, the image noise was lower than on the hybrid-IR image

Qualitative image analysis

Two board-certified radiologists (Y.N. and K.A. with 14 and 31 years of experience in radiology, respectively) performed consensual qualitative analysis of the CT images. They inspected a total of 276 scans (46 × 2 × 3) of 0.25 mm section thickness that were reconstructed with hybrid-IR, MBIR, and DLR. They were blinded to all patient demographics and CT parameters. The images were presented in random order on a preset soft tissue window; the window width and level were 300 and 60 HU, respectively.

The readers were given standardized instructions and trained on image sets from five patients not included in this study. They ranked the images obtained from the 46 patients for vessel conspicuity (visibility of small structures, especially the depiction of the segmental branch level of the hepatic artery) on HAP images and for overall image quality on HAP and EP images. Vessel grading was on the 5-point Likert scale, where 1 = very poor, 2 = suboptimal, 3 = acceptable, 4 = above average, and 5 = excellent [25]. The overall image quality was also scored on the 5-point Likert scale [26, 27], where 1 = unacceptable diagnostic image quality, 2 = subdiagnostic, 3 = average, 4 = above average, and 5 = excellent [25].

Quantitative image analysis

Quantitative analysis of transverse images (section thickness 0.25 mm) was performed by one radiologist (M.A. with

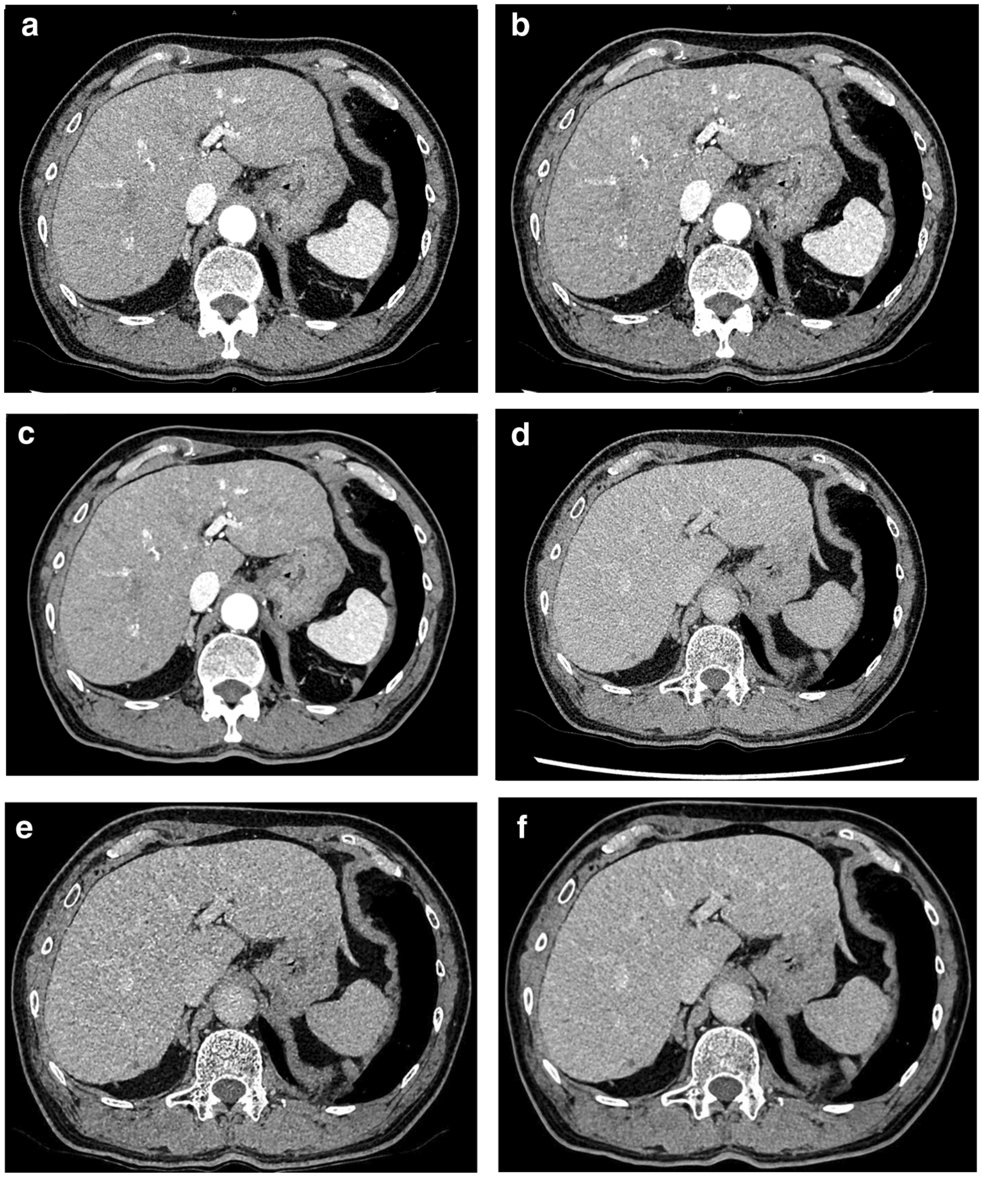

Fig. 3 Hepatic arterial (**a**–**c**) and equilibrium phase images (**d**–**f**) of a 76-year-old man. Reconstruction was with hybrid-IR (**a**, **d**), MBIR (**b**, **e**), and DLR (**c**, **f**). The image noise was lower on the DLR image than on the other images

5 years of experience in radiology). For attenuation measurements, regions of interest (ROIs) were placed within the aorta, portal vein, liver, and paraspinal muscle. Aortic attenuation was recorded at the celiac artery level using a single, manually drawn ROI as large as the vessel lumen; it avoided calcifications and/or soft plaques on the aortic wall. Portal vein attenuation was also recorded based on a single, hand-drawn ROI placed at the right and left portal vein confluence level. Liver attenuation was recorded as the mean measurement value of 4 ROIs in the right anterior, right posterior, left medial, and left lateral segment of the liver. Areas of focal changes in hepatic parenchymal attenuation, large vessels, and prominent artifacts, if any, were carefully avoided. Attenuation of the paraspinal muscle was recorded, also avoiding macroscopic fat infiltration, at the level of the right portal vein. Each value was calculated by averaging the three time measurements. The standard deviation (SD) of attenuation measured in the paraspinal muscle was used as the image noise.

For each of the image sets, the aortic, portal vein, and liver contrast-to-noise ratio (CNR), relative to the muscle, was calculated using the equation:

$$\mathrm{CNR} = (\mathrm{ROI}_{\mathrm{ORGAN}} - \mathrm{ROI}_{\mathrm{MUSCLE}})/N,$$

where $\mathrm{ROI}_{\mathrm{ORGAN}}$ is the mean attenuation of the organ of interest, $\mathrm{ROI}_{\mathrm{MUSCLE}}$ the mean attenuation of the paraspinal muscle, and N is the noise.

Statistical analysis

Statistically significant differences were evaluated with JMP10 software (SAS Institute). Differences among CT images subjected to hybrid-IR, MBIR, and DLR were determined. The two-sided Wilcoxon signed rank test with Bonferroni correction was applied to examine intergroup differences. Differences of $p < 0.013$ for multiple comparisons using Bonferroni correction were considered statistically significant.

For qualitative analysis, we calculated interobserver agreement using the weighted kappa statistic to evaluate agreement between the two readers. A kappa statistic in the range of 0.81–1.00 was interpreted as excellent, 0.61–0.80 as substantial, 0.41–0.60 as moderate, 0.21–0.40 as fair, and 0.00–0.20 as poor agreement [28].

Results

Quantitative analysis of the image noise and CNR

As shown in Table 1, image noise was much lower on DLR than hybrid-IR and MBIR images at HAP (median image noise was 24.9, 22.2, and 13.9 HU for hybrid-IR, MBIR, and DLR images, respectively; $p < 0.01$ for both), while there was a little difference between hybrid-IR and MBIR images (median image noise was 24.9 and 22.2 HU for hybrid-IR and MBIR images, respectively; $p < 0.01$). On EP images, DLR also yielded significantly lower image noise than hybrid-IR and MBIR (median image noise was 25.5, 23.1, and 14.6 HU for hybrid-IR, MBIR, and DLR images, respectively; $p < 0.01$ for both); it was lower on MBIR than hybrid-IR images (median image noise was 25.5 and 23.1 HU for hybrid-IR and MBIR images, respectively; $p < 0.01$). While there was a little difference in attenuation value of each organ among three reconstruction methods both on HAP and EP images (Supplemental Table 1), the aortic, portal vein, and liver CNR was significantly higher with DLR than the other reconstruction methods both on HAP and EP images ($p < 0.01$). The difference for liver CNR on HAP images and the aortic, portal vein, and liver CNR on EP images between hybrid-IR and MBIR images was not significant.

Qualitative analysis

DLR showed the highest overall image scores, and MBIR the lowest scores for both HAP and EP images (Table 2, Figs. 2, 3, and 4). All DLR images had a score of 3 (average) or higher in terms of overall image quality. On the other hand, 17.4% of hybrid-IR and 43.5% of MBIR images were subdiagnostic (score = 2) at HAP. This was true for 34.8% of hybrid-IR and 76.1% of MBIR images at EP. For vessel conspicuity, MBIR images yielded the highest scores; the scores for DLR and hybrid-IR images were comparable (Fig. 5). Interobserver agreement between the two readers was substantial (kappa value range 0.71–0.80).

Radiation exposure

The median $CTDI_{vol}$, DLP, and SSDE values for hepatic dynamic scans were 12.6 mGy (range 9.7–16.1), 1240.5 mGy cm (range 910.7–1950.5), and 17.7 mGy (range 15.6–20.4), respectively. They were slightly lower compared to conventional hepatic dynamic CT reported as the Japanese diagnostic reference levels [29].

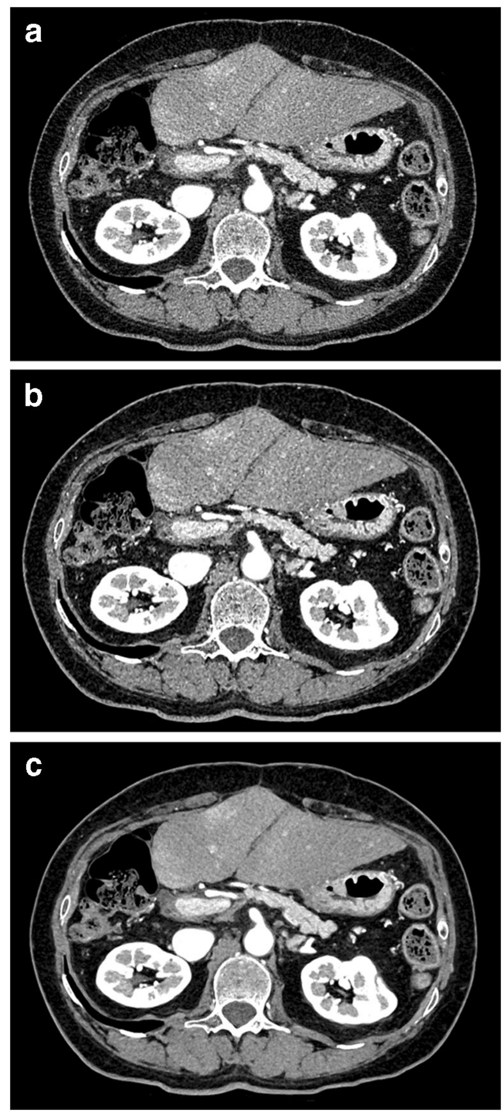

Fig. 4 Hepatic arterial phase images of a 59-year-old man. Reconstruction was with hybrid-IR (**a**), MBIR (**b**), and DLR (**c**). The image noise on the DLR image was markedly lower than on the other images. Note the improvement of image quality and better delineation not only for the liver but also other organs such as the pancreas and kidney on DLR image compared with hybrid-IR and MBIR images

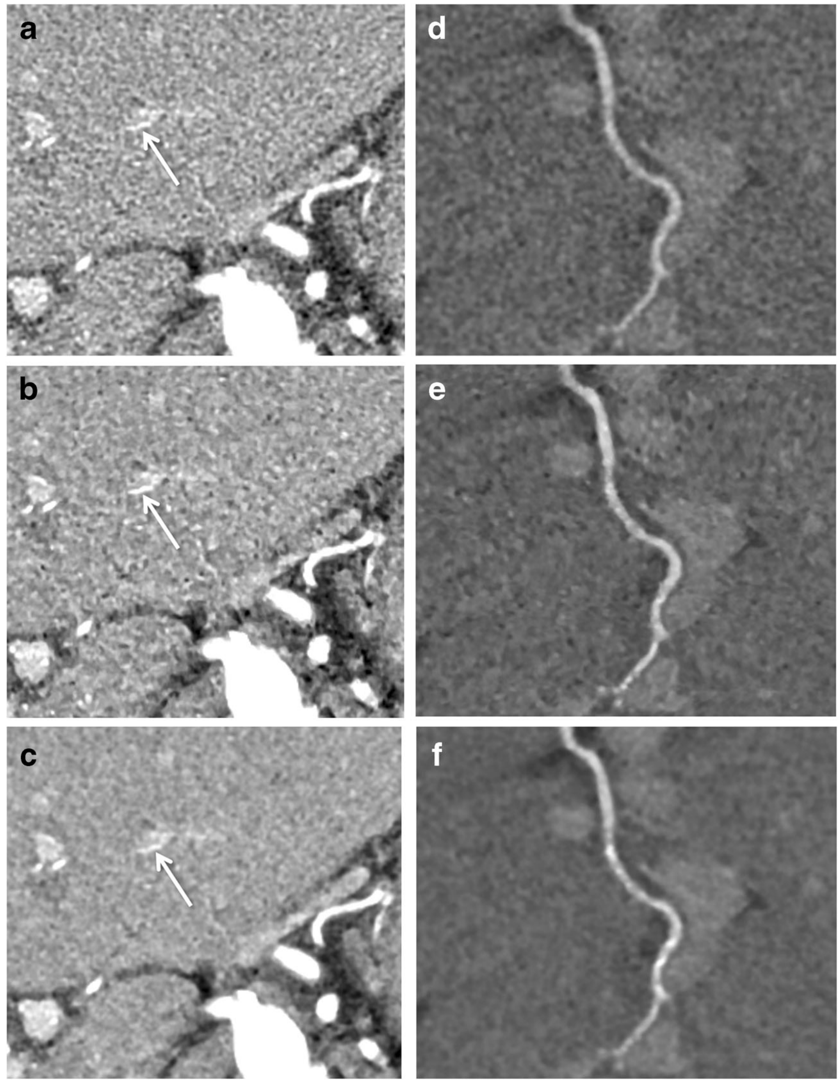

Fig. 5 Hepatic arterial phase images of an 81-year-old woman. Axial (**a**–**c**) and curved multiplanar reformation (CPR) images (**d**–**f**). Reconstruction was with hybrid-IR (**a**, **d**), MBIR (**b**, **e**), and DLR (**c**, **f**). On the hybrid-IR and DLR images, the branch level of the hepatic artery (arrow) was visualized, but the vascular edge was blurred and irregular; it was sharp on the MBIR image

Discussion

We found that DLR yielded a significantly lower image noise and higher CNRs than hybrid-IR and MBIR at both HAP and EP. The subjective overall image quality score was significantly better with DLR than hybrid-IR and MBIR. Thus, we concluded that DLR can yield better image quality than hybrid-IR and MBIR.

Although a reduction in the slice thickness degrades image quality, we selected 0.25 mm, the thinnest, to maximize the spatial resolution on these scans [30, 31]. In addition, image noise was higher on U-HRCT than conventional HRCT images due to the smaller size of the detectors [1, 4]. Thus, our protocol, thin slice images using U-HRCT, results in worse image quality due to increased noise as compared to conventional images. Indeed, hybrid-IR and MBIR images were graded as subdiagnostic (overall image quality score of 2 or lower) for some cases (between 17.4 and 76.1%). On the other hand, overall image quality score of 3 (average) or higher was assigned for all DLR images for all cases. Based on our findings, we suggest that as DLR allows thinner slices in abdominal U-HRCT images while maintaining image quality, DLR appears as an essential reconstruction method for U-HRCT scanning.

MBIR images yielded significantly lower image noise than hybrid-IR. However, MBIR resulted in the lowest scores among the three reconstruction methods for overall image quality. As determination of the SD is easy and quick, it is widely used to estimate the image noise on CT scans [32, 33]. However, it yields a very limited description of the noise characteristics because two images with very different noise textures may exhibit an identical SD [34]. MBIR is able to reduce many of the high-frequency but not the low-frequency noise components [9–11]. Therefore, we supposed that their qualitative image quality was not improved on MBIR images because the low-frequency noise components were not reduced.

In our study, vessel conspicuity was better on MBIR than hybrid-IR and DLR images. MBIR yields better visualization of small vessels than hybrid-IR because it reduces image noise while maintaining image contrast and resolution [16, 25, 35]. The DLR algorithm we applied was developed for abdominal images and not optimized for the evaluation of vessels. Thus, we think that DLR used in this study and MBIR are complementary for U-HRCT of the abdomen. Different DLR algorithms might be needed for the evaluation of vessels.

There was a significant difference in attenuation value of each organ among the three reconstruction methods although the difference was small. Regarding the attenuation value of aorta at HAP, for which the largest difference was observed, MBIR showed the highest value (about 10 HU higher compared to both hybrid-IR and DLR) as already reported [36, 37]. However, DLR yielded the higher CNR compared to the other two reconstruction methods for all organs including the aorta at both phases, indicating that noise reduction with DLR may overcome the difference in attenuation value of each organ.

Although the radiation exposure must be scrutinized [38], dose reduction must be balanced against an acceptable level of diagnostic accuracy. According to Pickhardt et al [12], the ability to detect focal hepatic lesions was reduced on low-dose MBIR images. DCNN for DLR was trained with MBIR images acquired with a sufficient radiation dose. To ascertain the ability to detect focal hepatic lesions on low-dose DLR images, further studies are needed.

Our study has some limitations. The study population was relatively small, and our investigation was retrospective and carried out at a single institution. Therefore, we consider our findings preliminary. We enrolled 46 patients although only 20 were required based on the power calculation. Very large samples may reject null hypotheses with clinically negligible differences, leading that what is insignificant may become significant [39]. However, the difference in image noise between DLR and other algorithms was larger compared to standard deviation of image noise of each reconstruction method, indicating that a significant difference in our data was not clinically negligible even though patient population was slightly larger compared to the required one based on the power calculation. Also, to avoid excessive radiation doses [29], PVP images of our patients were not performed in super-high-resolution mode and, consequently, were not included in this study. However, as PVP imaging is important for the evaluation of hypovascular hepatic metastases and of abnormalities of the portal venous system [40], further studies including PVP images are needed. We did not specifically evaluate focal hepatic lesions, which should be done. Finally, there is no external and further investigation including a larger cohort study and a phantom study is certainly needed.

In conclusion, image noise, overall image quality, and CNR for hepatic U-HRCT images improved with DLR compared to hybrid-IR and MBIR. Thus, DLR can improve abdominal CT image quality using U-HRCT.

Funding Dr. Kazuo Awai received a research funding from Canon Medical Systems Co. Ltd.

Compliance with ethical standards

Guarantor The scientific guarantor of this publication is Dr. Kazuo Awai.

Conflict of interest The authors of this manuscript declare relationships with the following companies: Canon Medical Systems Co. Ltd. for Kazuo Awai and Naruomi Akino and Canon Medical Research USA for Jian Zhou and Zhou Yu. Naruomi Akino, Jian Zhou, and Zhou Yu contributed to this study for manuscript editing regarding the description of deep learning reconstruction (DLR) algorithm. The authors who are not employees of Canon Medical Systems had control of inclusion of any data and information that might present a conflict of interest for those authors who are employees of Canon Medical Systems. The other authors declare that they have no conflict of interest.

Statistics and biometry No complex statistical methods were necessary for this paper.

Informed consent Written informed consent was not required for this study because this study used existing CT images including raw data.

Ethical approval Institutional Review Board approval was obtained.

Methodology
- retrospective
- diagnostic study
- performed at one institution

References

1. Kakinuma R, Moriyama N, Muramatsu Y et al (2015) Ultra-high-resolution computed tomography of the lung: image quality of a prototype scanner. PLoS One 10:e0137165
2. Motoyama S, Ito H, Sarai M et al (2018) Ultra-high-resolution computed tomography angiography for assessment of coronary artery stenosis. Circ J. https://doi.org/10.1253/circj.CJ-17-1281
3. Tanaka R, Yoshioka K, Takagi H, Schuijf JD, Arakita K (2018) Novel developments in non-invasive imaging of peripheral arterial disease with CT: experience with state-of-the-art, ultra-high-resolution CT and subtraction imaging. Clin Radiol. https://doi.org/10.1016/j.crad.2018.03.002
4. Yanagawa M, Hata A, Honda O et al (2018) Subjective and objective comparisons of image quality between ultra-high-resolution CT and conventional area detector CT in phantoms and cadaveric human lungs. Eur Radiol. https://doi.org/10.1007/s00330-018-5491-2
5. Nakayama Y, Awai K, Funama Y et al (2005) Abdominal CT with low tube voltage: preliminary observations about radiation dose, contrast enhancement, image quality, and noise. Radiology 237:945–951
6. Volders D, Bols A, Haspeslagh M, Coenegrachts K (2013) Model-based iterative reconstruction and adaptive statistical iterative reconstruction techniques in abdominal CT: comparison of image quality in the detection of colorectal liver metastases. Radiology 269:469–474
7. Chang W, Lee JM, Lee K et al (2013) Assessment of a model-based, iterative reconstruction algorithm (MBIR) regarding image

quality and dose reduction in liver computed tomography. Invest Radiol 48:598–606
8. Fontarensky M, Alfidja A, Perignon R et al (2015) Reduced radiation dose with model-based iterative reconstruction versus standard dose with adaptive statistical iterative reconstruction in abdominal CT for diagnosis of acute renal colic. Radiology 276:156–166
9. Nishizawa M, Tanaka H, Watanabe Y, Kunitomi Y, Tsukabe A, Tomiyama N (2015) Model-based iterative reconstruction for detection of subtle hypoattenuation in early cerebral infarction: a phantom study. Jpn J Radiol 33:26–32
10. Euler A, Stieltjes B, Szucs-Farkas Z et al (2017) Impact of model-based iterative reconstruction on low-contrast lesion detection and image quality in abdominal CT: a 12-reader-based comparative phantom study with filtered back projection at different tube voltages. Eur Radiol 27:5252–5259
11. Racine D, Ba AH, Ott JG, Bochud FO, Verdun FR (2016) Objective assessment of low contrast detectability in computed tomography with channelized Hotelling observer. Phys Med 32:76–83
12. Pickhardt PJ, Lubner MG, Kim DH et al (2012) Abdominal CT with model-based iterative reconstruction (MBIR): initial results of a prospective trial comparing ultralow-dose with standard-dose imaging. AJR Am J Roentgenol 199:1266–1274
13. Yasaka K, Furuta T, Kubo T et al (2017) Full and hybrid iterative reconstruction to reduce artifacts in abdominal CT for patients scanned without arm elevation. Acta Radiol 58:1085–1093
14. Nakamoto A, Kim T, Hori M et al (2015) Clinical evaluation of image quality and radiation dose reduction in upper abdominal computed tomography using model-based iterative reconstruction; comparison with filtered back projection and adaptive statistical iterative reconstruction. Eur J Radiol 84:1715–1723
15. Deak Z, Grimm JM, Treitl M et al (2013) Filtered back projection, adaptive statistical iterative reconstruction, and a model-based iterative reconstruction in abdominal CT: an experimental clinical study. Radiology 266:197–206
16. Higaki T, Tatsugami F, Fujioka C et al (2017) Visualization of simulated small vessels on computed tomography using a model-based iterative reconstruction technique. Data Brief 13:437–443
17. Cohen J (1988) Statistical power analysis for the behavior sciences (2nd ed.) Lawrence Erlbaum Associates, Hillsdale, NJ
18. Bruix J, Sherman M (2011) Management of hepatocellular carcinoma: an update. Hepatology 53:1020–1022
19. Bruix J, Sherman M (2005) Management of hepatocellular carcinoma. Hepatology 42:1208–1236
20. Lim JH, Choi D, Park CK, Lee WJ, Lim HK (2006) Encapsulated hepatocellular carcinoma: CT-pathologic correlations. Eur Radiol 16:2326–2333
21. American College of Radiology (2018) CT/MRI LI-RADS v2018 CORE. https://www.acr.org/Clinical-Resources/Reporting-and-Data-Systems/LI-RADS/CT-MRI-LI-RADS-v2018
22. Brady SL, Kaufman RA (2012) Investigation of American Association of Physicists in Medicine report 204 size-specific dose estimates for pediatric CT implementation. Radiology 265:832–840
23. Christner JA, Braun NN, Jacobsen MC, Carter RE, Kofler JM, McCollough CH (2012) Size-specific dose estimates for adult patients at CT of the torso. Radiology 265:841–847
24. American Association of Physicists in Medicine (2011) Size-specific dose estimates (SSDE) in pediatric and adult body CT examinations (Task Group 204). American Association of Physicists in Medicine, College Park. Available via https://www.aapm.org/pubs/reports/RPT_204.pdf. Accessed on 22 February 2019
25. Hur BY, Lee JM, Joo I et al (2014) Liver computed tomography with low tube voltage and model-based iterative reconstruction algorithm for hepatic vessel evaluation in living liver donor candidates. J Comput Assist Tomogr 38:367–375
26. Phelps AS, Naeger DM, Courtier JL et al (2015) Pairwise comparison versus Likert scale for biomedical image assessment. AJR Am J Roentgenol 204:8–14
27. Likert R (1932) A technique for the measurement of attitudes. Arch Psychol 140:55
28. Svanholm H, Starklint H, Gundersen HJ, Fabricius J, Barlebo H, Olsen S (1989) Reproducibility of histomorphologic diagnoses with special reference to the kappa statistic. APMIS 97:689–698
29. Japan Association on Radiological Protection in Medicine (2015) Diagnostic reference levels based on latest surveys in Japan: Japan DRLs 2015. Available via http://www.radher.jp/J-RIME/report/DRLhoukokusyoEng.pdf. Accessed on 22 February 2019
30. Yoshioka K, Tanaka R, Takagi H et al (2018) Ultra-high-resolution CT angiography of the artery of Adamkiewicz: a feasibility study. Neuroradiology 60:109–115
31. Tamm EP, Rong XJ, Cody DD, Ernst RD, Fitzgerald NE, Kundra V (2011) Quality initiatives: CT radiation dose reduction: how to implement change without sacrificing diagnostic quality. Radiographics 31:1823–1832
32. Goldman LW (2007) Principles of CT: radiation dose and image quality. J Nucl Med Technol 35:213–225 quiz 226-218
33. Lubner MG, Pickhardt PJ, Tang J, Chen GH (2011) Reduced image noise at low-dose multidetector CT of the abdomen with prior image constrained compressed sensing algorithm. Radiology 260:248–256
34. Friedman SN, Fung GS, Siewerdsen JH, Tsui BM (2013) A simple approach to measure computed tomography (CT) modulation transfer function (MTF) and noise-power spectrum (NPS) using the American College of Radiology (ACR) accreditation phantom. Med Phys 40:051907
35. Kaza RK, Platt JF, Goodsitt MM et al (2014) Emerging techniques for dose optimization in abdominal CT. Radiographics 34:4–17
36. Scheffel H, Stolzmann P, Schlett CL et al (2012) Coronary artery plaques: cardiac CT with model-based and adaptive-statistical iterative reconstruction technique. Eur J Radiol 81:e363–e369
37. Hajdu SD, Daniel RT, Meuli RA, Zerlauth JB, Dunet V (2018) Impact of model-based iterative reconstruction (MBIR) on image quality in cerebral CT angiography before and after intracranial aneurysm treatment. Eur J Radiol 102:109–114
38. Mathews JD, Forsythe AV, Brady Z et al (2013) Cancer risk in 680,000 people exposed to computed tomography scans in childhood or adolescence: data linkage study of 11 million Australians. BMJ 346:f2360
39. Faber J, Fonseca LM (2014) How sample size influences research outcomes. Dental Press J Orthod 19:27–29
40. Soyer P, Poccard M, Boudiaf M et al (2004) Detection of hypovascular hepatic metastases at triple-phase helical CT: sensitivity of phases and comparison with surgical and histopathologic findings. Radiology 231:413–420